Numerical study of momentum and energy transfer in the interaction of a laser pulse carrying orbital angular momentum with electrons

V.T. Tikhonchuk, Ph. Korneev, E. Dmitriev, R. Nuter

Version of Record: https://www.sciencedirect.com/science/article/pii/S1574181820301002
Manuscript_5da743c9b3467fbb49313389f62bf223

Numerical study of momentum and energy transfer in the interaction of a laser pulse carrying orbital angular momentum with electrons

V.T. Tikhonchuk[a,b,*], Ph. Korneev[c,d], E. Dmitriev[c,d], R. Nuter[a]

[a] *CELIA, University of Bordeaux, CNRS, CEA, 33405 Talence, France*
[b] *ELI-Beamlines, Institute of Physics, Czech Academy of Sciences, 25241 Dolní Břežany, Czech Republic*
[c] *National Research Nuclear University "MEPhI" (Moscow Engineering Physics Institute), Moscow, 115409 Russia*
[d] *P. N. Lebedev Physics Institute, Russian Academy of Sciences, 119991 Moscow, Russia*

Abstract

Electromagnetic waves, in addition to the energy and momentum, can also carry an orbital angular momentum (OAM). Transfer of these quantities from laser to particles may find various applications. There are similarities between the process of OAM transfer from laser to electrons and a direct electron acceleration in a relativistic electromagnetic wave packet. In this paper, by using a numerical integration of electron's equation of motion, we present a general analysis of the energy and momentum transfer from a laser wave packet carrying orbital angular momentum to electrons. The theoretical model demonstrates that relation between the transfer of the axial and orbital angular momenta from laser to electrons depends strongly on the laser waveform and polarization.

Keywords: electromagnetic waves, orbital angular momentum, direct laser acceleration

1. Introduction

Electromagnetic waves carrying an orbital angular momentum (OAM) were introduced by Allen et al. [1] and rapidly found various applications in optics for compact information storage and nanoscale imaging and manipulation [2]. Such waves have a form of radially limited beams described by Laguerre–Gaussian functions, which are eigenmodes of the paraxial optics equation in the cylindrical coordinates. Such laser beams can also find applications in the domain of relativistic intensities, where laser field more efficiently interacts with collective plasma excitations or with individual electrons. Recent publications show that interaction of such relativistic electromagnetic beams in plasma may excite large

*Corresponding author
Email address: tikhonchuk@u-bordeaux.fr (V.T. Tikhonchuk)

amplitude plasma waves, transfer to electrons a part of their orbital momentum, and create quasistatic magnetic fields [3, 4, 5, 6, 7, 8, 9].

These processes have many features in common with the direct acceleration of electrons in relativistic laser wave packets [10, 11, 12]. According to the Lawson–Woodward theorem [13, 14], a charged particle cannot gain energy and momentum while interacting with a plane electromagnetic wave. A transfer, however, becomes possible if the wave packet has a finite duration, finite radial extent or presents a spatio-temporal coupling. A particle is then displaced under the action of the ponderomotive force, the phase relation is detuned, which opens a possibility for an energy and momentum transfer. This effect, however, is weak in a small amplitude wave, where the particle motion is non-relativistic and displacement is of a second order on the wave amplitude. Much more efficient particle acceleration is expected in the relativistic regime, where particle attains a relativistic velocity and could enter in phase resonance with the electromagnetic wave.

In this paper, we extend the problem of single particle interaction with an electromagnetic wave to the case of wave packets carrying an orbital angular momentum and show how such properties of the wave packet as the mode structure, polarization and chirp may significantly affect the efficiency of momentum transfer. We integrate the equation of motion of an electron initially at rest with distributed initial positions, and evaluate the average momentum and energy gain. It is found that by changing the wave polarization and by introducing a angular-temporal coupling in the laser pulse, one can significantly enhance the orbital momentum transfer compared to the axial momentum and energy transfer. This process is manifested itself by generation of a strong axial magnetic field at a kilotesla level, which can be obtained with available high power short-pulse lasers.

Compared to the full kinetic particle-in-cell (PIC) simulations, a single particle approach is simpler and it allows to explore a broader range of laser pulse parameters, but it cannot account for the self-consistent fields in plasma arising from electron motion and charge separation between electrons and ions. By contrast, it allows to trace the origin of the orbital angular momentum transfer, which is due to the spatial and phase gradients of the applied field. Collective effects contribution is proportional to the plasma density and it can be evaluated in the complementary PIC simulations, which are out of scope of this paper. However, the presented results are qualitatively valid for a low-density plasma, where the laser field is not considerably perturbed.

2. Equations for the waves and the particles

Electron motion in the laser field is described by dynamic equations for the electron momentum $\mathbf{p}$ and the coordinate $\mathbf{r}$:

$$d_t\mathbf{p} = -e\mathbf{E} - e\mathbf{v}\times\mathbf{B}, \qquad d_t\mathbf{r} = \mathbf{v}, \tag{1}$$

where $\mathbf{v} = \mathbf{p}/m_e\gamma$ is the electron velocity and $\gamma = (1 + \mathbf{p}^2/m_e^2c^2)^{1/2}$ is the relativistic factor, e is the unitary charge, m_e is the electron mass and c is

the light velocity. The particle orbital moment $l_z = rp_\theta$ is defined in polar coordinates with respect to the laser propagation axis z. In what follows we use the relativistic units where time is normalized by the laser frequency ω, length by the wave number $k = \omega/c$ and electric field by the Compton field $m_e\omega c/e$. The wave amplitude is assumed to be relativistic but not too high ($\lesssim 10^{20}$ W/cm^2) so that the radiation friction could be neglected.

We consider a laser beam with transverse electric field represented in the paraxial approximation as a linear combination of the Laguerre-Gaussian modes:

$$E_{\rm las} = \sum_{p,l} E_{p,l} \frac{w_0}{w_b} F_{p,l}\left(\frac{r^2}{w_b^2}\right) \cos(l\theta + \varphi_{p,l}), \tag{2}$$

where $E_{p,l}$ is the mode amplitude, r and θ are polar coordinates in x, y plane and function $F_{p,l}$ describes the beam shape in the transverse plane:

$$F_{p,l}(X) = \sqrt{\frac{p!}{(|l|+p)!}} X^{|l|/2} L_p^{|l|}(X)\, \mathrm{e}^{-X/2}.$$

Here $L_p^{|l|}(X)$ is a generalized Laguerre polynomial of degrees p and l. The set of functions $F_{p,l}(X)$ is orthogonal and normalized. The beam width $w_b(z) = w_0\sqrt{1 + z^2/z_R^2}$ and wave phase

$$\varphi_{p,l} = kz - \omega t + \frac{kzr^2}{2z_R w_b^2} - (2p + |l| + 1) \arctan\frac{z}{z_R}$$

account for the wave front curvature and Gouy phase. Here we consider the interaction within the Rayleigh length, $|z| \lesssim z_R = kw_0^2$, so the major dependence on the axial coordinate z enters in a combination, $z - ct$. The radial wave number $p \geq 0$ is an integer that numerates radial modes. The integer l could be positive or negative, and it numerates the orbital angular momentum (OAM). Other field components, both transverse and longitudinal, are obtained from the Maxwell equations within the paraxial approximation. Several examples of different field polarizations are considered below.

An electric field of a linearly polarized (LP) electromagnetic wave is defined as a special case of Eq. (2):

$$E_x = B_y = a(z)\, f(r)\, g(\tau)\, \cos(l\theta + \varphi_{p,l}), \tag{3}$$

where $a(z) = a_0 w_0/w_b(z)$, a_0 is the dimensionless wave amplitude in the focal point, $\tau = t - z/c - Ct_{\rm las}\theta/2\pi$ and $f(r) = F_{p,l}(r^2/w_b^2)$ is the radial mode function. The time envelope function $g(\tau)$ describes temporal shape of the wave packet with a parameter C characterizing an angular-temporal coupling. Other polarizations are defined in a standard way as a linear combination of E_x and E_y. Optical beams with $C \neq 0$ were introduced by Pariente and Quéré [15] and called "light springs". They are discussed in detail in Sec. 3.3. In calculations, we consider a sine-like envelope: $g(\tau) = \sin(\pi\tau/t_{\rm las})$ defined in the interval

$0 < t < t_{\rm las}$. In that case, laser pulse carries energy $W_{\rm las} = (\pi/4)a_0^2(kw_0)^2\omega t_{\rm las}$ and orbital momentum $L_{\rm las} = (\pi/4)la_0^2(kw_0)^2\omega t_{\rm las}$ in the relativistic units. The energy unit for the whole laser beam is $m_e^2c^5\epsilon_0/e^2\omega = n_c m_e c^5/\omega^3$, where ϵ_0 is the vacuum dielectric permittivity and $n_c = m_e\omega^2\epsilon_0/e^2$ is the critical density. The orbital momentum unit is $m_e^2c^5\epsilon_0/e^2\omega^2$. As a reference, these units correspond for laser wavelength of $1\,\mu$m, to an energy unit of $0.367\,\mu$J and an orbital momentum unit of 1.94×10^{-22} J·s $= 1.84\times10^{12}\hbar$. Thus, quantum effects have no importance.

A pulse of a circular polarization (CP) is defined in polar coordinates as follows

$$E_r = B_\theta = 2^{-1/2}a(z)\,f(r)\,g(\tau)\,\cos[(l+s)\theta+\varphi_{p,l}], \qquad (4)$$
$$E_\theta = -B_r = -2^{-1/2}s\,a(z)\,f(r)\,g(\tau)\,\sin[(l+s)\theta+\varphi_{p,l}].$$

It carries, in addition to the orbital momentum, a spin momentum with $s = \pm1$ defining the sense of field rotation. Thus the total orbital momentum is sum of the orbital and spin momentum, $L_{\rm las} = (\pi/4)(l+s)a_0^2(kw_0)^2\omega t_{\rm las}$.

Following the paper [8], we also consider a special case of electric field vector rotating with the polar angle:

$$E_r = B_\theta = a(z)\,f(r)\,g(\tau)\,\cos\alpha\,\cos(l\theta+\varphi_{p,l}), \qquad (5)$$
$$E_\theta = -B_r = -a(z)\,f(r)\,g(\tau)\,\sin\alpha\,\cos(l\theta+\varphi_{p,l}),$$

where α is an angle of the electric field vector with respect to the radius. The case $\alpha = 0$ corresponds to the radial polarization (RP) and $\alpha = \pi/2$ to the azimuthal polarization. (Below, we use generic abbreviation RP for cases with arbitrary angle α.) This wave packet is not an exact solution of the paraxial equation, it can be considered as a linear combination of two circularly polarized modes of an opposite sense of rotation, with orbital moments $l\pm1$ shifted in time by a phase 2α and having the radial structure corresponding to the p, l mode [16]. It carries the same energy and orbital momentum as a linearly polarized pulse.

As we are interested in tightly focused pulses, it is important to account for the axial components of electric and magnetic field, which are calculated from the condition of zero divergence in the first paraxial approximation:

$$\partial_z E_z = -\partial_x E_x - \partial_y E_y, \qquad \partial_z B_z = -\partial_x B_x - \partial_y B_y. \qquad (6)$$

Explicit expressions for the axial components of electric and magnetic fields are given in Appendix A.

3. Numerical calculations of the particle dynamics

Electron dynamics in the wave packets described above is evaluated by solving numerically equations of motion (1) assuming that electrons are initially at rest and homogeneously distributed in the laser focal plane $z = 0$. Typically several hundred thousand test particles have been considered for a given

set of parameters. We calculate the components of momentum p_r, p_θ and p_z, the orbital moment with respect to the laser beam axis, $l_z = rp_\theta$, and energy $\varepsilon = (1 + p_r^2 + p_\theta^2 + p_z^2)^{1/2} - 1$. At the end of laser pulse these parameters are averaged over the initial azimuthal angle θ_0 for a given initial radius r_0. For example, the average energy reads:

$$\bar{\varepsilon}(r_0) = \frac{1}{2\pi} \int_0^{2\pi} d\theta_0 \, \varepsilon(\theta_0).$$

Then, a total energy and momentum transferred to a particle are evaluated by integrating over the initial radius r_0. For example, the total energy is calculated as follows:

$$\mathcal{E}_e = 2\pi \int_0^{r_{\max}} dr_0 \, r_0 \, \bar{\varepsilon}(r_0).$$

The value of upper limit $r_{\max} = 3w_0$ is sufficiently large so almost all particles that may interact with laser pulse are accounted for. The total energy and momentum transferred to plasma of density n_e and length z_p is calculated straightforwardly as $W_e = \mathcal{E}_e k z_p n_e / n_c$ and $L_e = L_z k z_p n_e / n_c$.

3.1. Linearly polarized laser beam

As a reference case, we consider a linearly polarized laser beam with the following set of parameters: $a_0 = 1$, $kw_0 = 15\pi$, $\omega t_{\text{las}} = 24\pi$, $p = 0$, $l = 1$ and $C = 0$. The total laser pulse energy in this case is: $W_{\text{las}} = L_{\text{las}} = 1.3 \times 10^5$, which corresponds to energy of 48 mJ and orbital angular momentum of 2.5×10^{-17} J·s for a 1 μm light. Figure 1 shows an example of radial dependence of electron angle-averaged radial (a), axial and orbital (b) momentum.

It follows from Eqs. (1) that in the first order paraxial approximation the dephasing factor $R = \varepsilon/c - p_z$ satisfies an equation

$$d_t R = eE_z(1 - v_z/c).$$

The right hand side is zero in a plane wave and therefore, $R = 0$ for a particle initially at rest [13, 14]. This law does not applies to a focused laser beam where the axial electric field is non-zero. However, we observe that for the considered set of parameters, there is a minor deviation from the wavefront planarity and the dephasing factor is conserved with a good precision if $C = 0$. This is not anymore true for laser pulses with spatio-temporal coupling, $C \neq 0$, as it is demonstrated in Sec. 3.3.

Radial component $\bar{p}_r \sim 0.1$ is the dominant part of electron momentum. It is produced by the radial component of the ponderomotive force, which dominates the interaction as it is of the first order of $1/kw_0$. This can be seen in Fig. 1, where the two maxima of radial momentum are shifted to the left and to the right from the position of the laser intensity maximum. Positive values of $\bar{p}_r$ for $kr > 40$ are due to electron acceleration outwards. Positive values of $\bar{p}_r$ near the axis, $kr \lesssim 40$, are related to electrons accelerated inwards and inverted their momentum while passing near the laser axis.

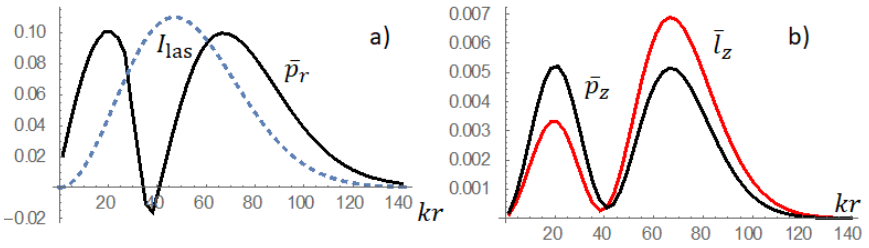

Figure 1: Radial dependence of the averaged characteristics of an electron acquired in the interaction with a linearly polarized laser pulse with the following parameters: $a_0 = 1$, $kw_0 = 15\pi$, $\omega t_{\rm las} = 24\pi$, $p = 0$, $l = 1$ and $C = 0$. a) Radial momentum (solid line) and laser pulse intensity (dashed line, in arbitrary units). b) Axial momentum (black) and orbital momentum (red).

The value of dephasing parameter in this case is rather small, $R \lesssim 10^{-5}$. Consequently, the electron energy and axial momentum are equal each other, $\bar{\varepsilon} \approx \bar{p}_z \sim 0.005$, and more than one order of magnitude smaller than $\bar{p}_r = 0.1$. Conservation of $R \approx 0$ provides a relation between the transverse and axial moments, $p_z \approx p_r^2/2$, which explains the observed smallness of energy gain. Consequently, the axial and azimuthal moments appear at the second order on the paraxial parameter. They take non-zero values only due to the radial displacement of the particle and its acceleration in the axial electric field.

Figure 1 exhibits a good correlation between the axial and orbital momenta. They show very similar radial dependence and are equal to each other within $20 - 30\%$ (in dimensionless units). This is not evident beforehand, as they are controlled by different components of electric and magnetic field. Nevertheless, this is an indication that they are of the same nature – a partial resonance between the particle and the laser electric field. A similarity between the processes of axial and azimuthal acceleration is further demonstrated by the scaling of the total momentum transfer with the laser amplitude in Fig. 2.

The total radial momentum P_r scales approximately as square of laser amplitude in the non-relativistic limit, $a_0 < 1$, while the growth slows down at higher amplitudes. This behavior is compatible with dependence of the ponderomotive potential on laser amplitude, which for a linearly polarized field is $\sqrt{1 + a_0^2/2} - 1$. It is verified in the simulations (not shown in the figure), that the radial momentum scales linearly with laser pulse duration and inversely proportional to the beam width for a given amplitude. Laser orbital momentum does not have notable effect on the radial momentum transfer to electrons. Indeed, azimuthal dependence disappears when the square of laser field in Eq. (3) is averaged over the laser period. That fact indicates also that in addition to the laser ponderomotive force, the direct interaction with the laser electric field contributes to the axial and azimuthal electron acceleration as it was already discussed in Refs. [11, 12].

Dependence of the axial and orbital momenta on laser amplitude is much stronger, it scales approximately as laser amplitude in a power of three in the

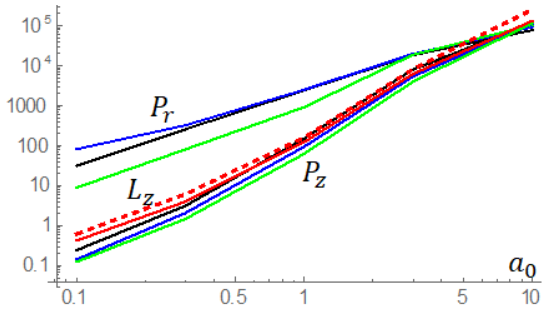

Figure 2: Dependence of the total momentum gained by an electron in the interaction with a linearly polarized (LP) laser pulse on an amplitude a_0 for the following parameters: $kw_0 = 15\pi$, $\omega t_{\rm las} = 24\pi$, $p = 0$ and $C = 0$. Black, blue and green lines show the radial P_r and axial P_z momentum for $l = 0$, 1 and 2, respectively. Red lines show the orbital momentum for $l = 1$ (solid line) and $l = 2$ (dashed line). The data for this figure are presented in Appendix B in Tab. B.2.

considered parameter range: P_z and L_z are approximately equal to each other, and their values depend weakly on the orbital number l for the same other parameters. Obviously, $L_z = 0$ for $l = 0$, but transfer of OAM from laser beams with $l = 1$ and $l = 2$ differs by less than $30 - 50\%$, while transfer of axial momentum P_z remains almost unchanged.

In the non-relativistic case, the axial and azimuthal momenta transfer to electron can be considered as a higher order process with respect to the radial acceleration, which itself is of a second order in the laser field amplitude. So, the efficiency of momentum transfer from laser to electrons is relatively small. For example, in a plasma of a density 1% of the critical density and a length of hundred wavelength, the efficiency of the axial momentum transfer in the considered example is 0.37% and 0.48% for the OAM transfer. The efficiency can be increased by increasing pulse duration and plasma length or tighter laser beam focusing. Moreover, by varying laser polarization and angular-temporal coupling it is possible to find configurations where orbital momentum transfer could be significantly increased.

3.2. Circularly and radially polarized laser beams

Circularly polarized (CP) laser beams are carrying spin in addition to orbital momentum, so even Gaussian beams with $l = 0$ may transfer some orbital momentum to electrons. But the nature of momentum transfer is different in this case of $l = 0$: as the most intense electric field is on the laser axis and the axial and orbital momenta are shifted closer to the axis. The total axial momentum transferred to electrons with a beam of circular polarization and $l = 0$ is approximately equal to the momentum transferred by a linearly polarized beam with $l = 0$, but in addition, an orbital momentum is transferred with a circularly polarized beam, $L_z \approx 64.7$. Results of several simulations of electron acceleration with a circularly polarized laser beam are presented in Tab. B.3 in Appendix B.

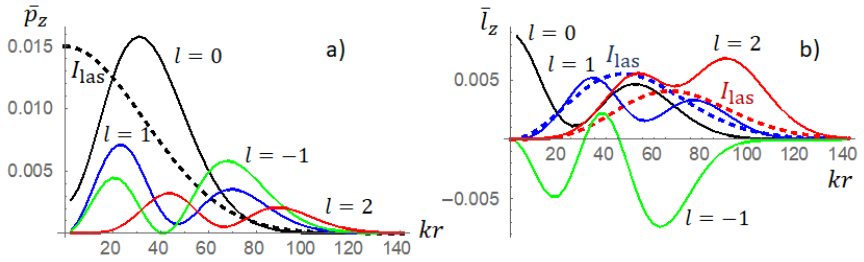

Figure 3: Radial dependence of the total axial (a) and orbital (b) momentum gained by electron in a circularly polarized (CP) laser beam with the following parameters: $a_0 = 1$, $kw_0 = 15\pi$, $\omega t_{\rm las} = 24\pi$, $p = 0$ and $C = 0$. Black lines show the case $l = 0$, blue lines $l = 1$, green lines $l = -1$ and red lines $l = 2$. Dashed lines show the laser intensity distribution for $l = 0$ (a, black) and for $l = 1$ and 2 (b, blue and red lines, respectively).

A circularly polarized beam with $l = 0$ transfers a smaller orbital momentum ($L_z \approx 64.7$) than a linearly polarized beam with $l = 1$ ($L_z \approx 125$), although they carry the same amount of orbital momentum. This is explained by the fact that laser beams in these two cases have different radial intensity distributions and hence couple to electrons at different distances from the axis. Figure 3 shows radial distribution of momenta for circularly polarized laser beams with orbital momentum varying from $l = -1$ to 2. Radial distributions of the axial and orbital momenta are rather different for $l = 0$: the former one has a maximum where the radial intensity gradient is the strongest (panel a), while the latter one has two maxima – near the axis and at the beam edge (panel b). A situation is rather different for OAM laser beams with $l = \pm 1$ and $l = 2$. The axial momentum has two maxima with a minimum between them coinciding with the laser intensity maximum. The orbital momentum for $l = 1$ has one maximum approximately coinciding with the intensity maximum, while for there are two maxima with a minimum coinciding with the intensity maximum. In contrast, by adding a negative orbital momentum $l = -1$ to a circularly polarized laser beam with $s = 1$ one may strongly suppress the OAM transfer and change its sign. In this case $P_z = 103$ and $L_z = -87.3$.

This analysis complements the results of numerical PIC simulations of electron acceleration with circularly polarized beams carrying OAM reported in Ref. [7], where the authors also observed increase of orbital momentum transfer with increasing orbital number.

Thus, by combining a circular polarization and orbital angular momentum one may vary the ratio of orbital to axial momentum transfer by a factor of 3. A particular case is a circularly polarized beam with $s = 1$ and $l = -1$. According to the laser orbital momentum definition, the beam does not carry the total orbital momentum and the electric field does not depend on the azimuthal angle. Nevertheless, the electric field rotates in time in each point of the beam and electrons are gaining a net negative orbital momentum, as shown in Fig. 3.

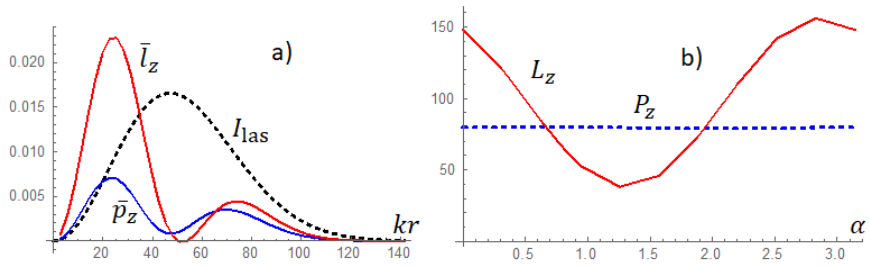

Figure 4: a) Radial dependence of the axial (blue) and orbital (red) momenta of electrons at the end of the laser pulse with a radially polarized (RP) electric field with $\alpha = 0$. b) Dependence of the average axial (dashed blue) and orbital (red line) final momentum gained by electron on the angle α. Both panels correspond to a radially polarized (RP) laser beam with the following parameters: $a_0 = 1$, $kw_0 = 15\pi$, $\omega t_{\rm las} = 24\pi$, $p = 0$, $l = 1$ and $C = 0$. Angle $\alpha = 0$ corresponds to the radially-oriented electric field, and $\alpha = \pi/2$ to the azimuthal orientation.

Laser beams of radial polarization (RP) with $\alpha \approx 0$ were considered in Ref. [8]. By using 3D PIC simulations, it was shown that tightly focused laser beam may transfer a significant amount of orbital momentum to electrons and produce a strong axial magnetic field lasting long after the pulse. We consider laser beams of radial and/or azimuthal polarization as given by Eq. (5) with the same energy, width and duration as in the previous cases of linearly and circularly polarized beams. Figure 4a shows a radial distribution of the axial and orbital momenta in a radially polarized (RP) beam ($\alpha = 0$) with all other parameters the same as in the reference case presented in Sec. 3.1. Compared to the case of linear polarization (LP) shown in Fig. 1b, the electron orbital momentum near the axis increases, thus resulting in overall increase of L_z by 20% while the electron axial momentum decreases by 20%.

Dependence of the average axial and orbital momentum of the angle α between the electric field vector and radius-vector is shown in Fig. 4b. The total axial momentum does not depend on the electric field orientation and it is 20% smaller than in the case of linear polarization. By contrast, orbital momentum varies significantly with angle α. The maximum orbital momentum transfer is achieved for a near radial polarization, while it is reduced about 4 times in the case of azimuthal polarization ($\alpha = \pi/2$). A similar dependence of the OAM transfer to electrons in a laser beam of radial, azimuthal and linear polarization is observed in numerical PIC simulations in Ref. [16].

3.3. Laser beams with spatio-temporal coupling

Stretching of laser pulse allows to extend the time of interaction of laser pulse with electrons while keeping the same local laser intensity and the same total laser pulse energy. Laser pulses with angular-temporal coupling carrying an orbital momentum, called "light springs", were proposed in Ref. [15] as a means for an increase of OAM transfer.

Figure 5 presents qualitatively intensity distribution of a laser pulse with orbital momentum $l = 1$ with and without spatio-temporal coupling. In the

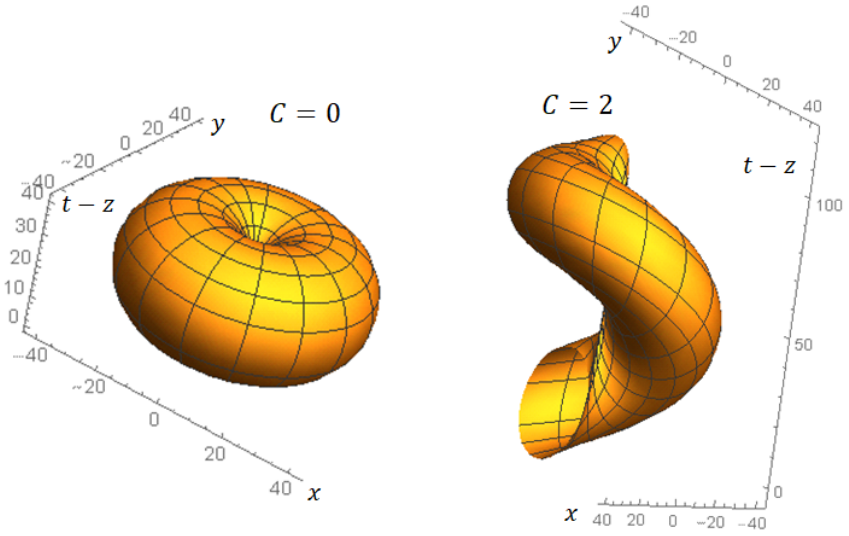

Figure 5: Spatio-temporal distribution of the intensity of a laser pulse with $l = 1$ and $C = 0$ (left) and $C = 2$ (right). Note the difference in scale in these two panels.

case $C = 0$, while the phase of the electric field depends on the azimuthal angle according to Eq. (3), the intensity distribution averaged over the laser period is azimuthally symmetric. The surface of constant intensity has a doughnut shape shown in the left panel in Fig. 5. By contrast, spatio-temporal coupling introduces the azimuthal asymmetry: while the pulse duration for any given azimuthal position remains the same, the pulse at larger angles arrives later in time. Thus, the intensity distribution takes a shape of a spiral, as shown in the right panel in Fig. 5.

It was demonstrated in Ref. [5] that the orbital momentum transfer indeed increases by using linearly polarized laser beams with angular-temporal coupling. The authors, however, considered the laser interaction with a plasma and assumed a resonance between the frequency chirp and the electron plasma frequency. Such a situation cannot be modeled in a single particle approach, nevertheless, stretching of laser pulse allows to an electron may to stay a longer time within laser field and to gain a larger azimuthal momentum. Our angular-temporal coupling parameter C corresponds to splitting of the laser frequency ω in two spectral components $\omega \pm \pi/t_{\mathrm{las}}$ and the laser orbital momentum l in two components $l \pm C/2$. It can be related to the spectral derivative of the orbital momentum $dl/d\omega$ introduced in Refs. [15, 5] by the following relation $dl/d\omega = Ct_{\mathrm{las}}/2\pi$.

We investigate the momentum transfer for chirped linearly, circularly and radially polarized laser beams. Results presented in Tab. 1 show strong variation of the electron orbital momentum while the radial and axial moments remain unchanged. For $C = \pm 2$, electrons are gaining more than ten times

C	$\mathcal{E}_e$	P_z	L_z LP	L_z CP	L_z RP
2.5	79.7	53.8	-1260	-929	2000
2.0	79.7	48.2	-873	-605	1590
1.5	79.7	60.7	-152	207	1200
1.0	79.7	75.4	310	414	835
0.5	79.7	79.1	332	393	490
0	96.0	96.0	125	144	148
-0.5	79.7	79.1	-110	48.1	143
-1.0	79.7	72.8	-13.5	99.2	-539
-1.5	79.7	55.9	529	766	-898
-2.0	79.7	45.4	1260	1700	-1290
-2.5	79.7	51.6	1570	2150	-1700

Table 1: Energy, axial and orbital momentum transfer for the case of linear (LP), circular (CP) and radial (RP) polarization for $a_0 = 1$, $kw_0 = 15\pi$, $\omega t_{\rm las} = 24\pi$, $p = 0$ and $l = 1$ for the chirp varying from $C = -2.5$ to $C = 2.5$. The energy and axial moments remain approximately the same in all considered cases.

larger orbital momentum compared to a non-stretched pulse. This is in striking difference from simple increasing of the laser pulse duration, which results in linear increase of all three moments with approximately constant relation between them. Moreover, the strongest orbital momentum transfer is found for a radially polarized beam. The effect is slightly less significant for a circular and linear polarization with an opposite sign of OAM.

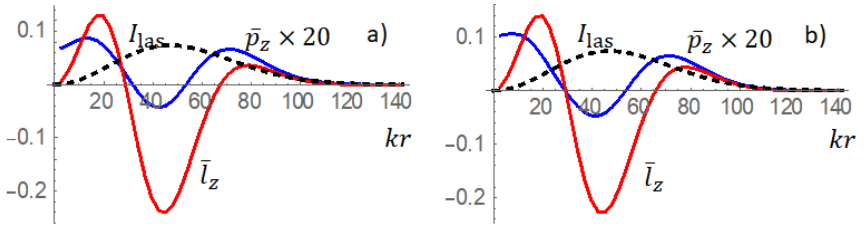

Figure 6: Radial dependence of the averaged axial (blue, multiplied by a factor of 20) and orbital (red) moment of electron after the end of a stretched laser pulse for the following parameters: $a_0 = 1$, $kw_0 = 15\pi$, $\omega t_{\rm las} = 24\pi$, $p = 0$, $l = 1$, $C = 2$. Linear (a) and circular (b) polarization. Dashed line shows a radial profile of the laser pulse in arbitrary units.

Radial distribution of particle axial and orbital momenta in Fig. 6 shows a correlation between them: electrons originating near the laser intensity maximum gain a largest in absolute value orbital momentum in the case of linear and circular polarization. The axial momentum is much smaller, it is multiplied by a factor of 20 in the figure for a better visibility. The magnitudes of axial and orbital moments are the same for all polarizations. These profiles are rather similar to the reference case with $C = 0$ shown in Fig. 1b, but with more than 20 times higher maxima for OAM.

This specific behavior can be understood by analyzing acceleration of elec-

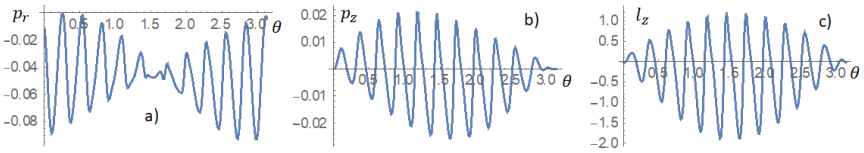

Figure 7: Dependence of the radial (a), axial (b) and orbital (c) electron moments after the end of a stretched laser pulse on the initial azimuthal angle for the initial radius $kr_0 = 40$ and the following laser parameters: $a_0 = 1$, $kw_0 = 15\pi$, $\omega t_{\rm las} = 24\pi$, $p = 0$, $l = 1$, $C = 2$, linear polarization.

trons at a particular distance from the axis. Figure 7 shows dependence of radial, axial and orbital moments on the initial azimuthal position of the particle for $kr = 40$, near the maximum of the amplitude. The average of these curves correspond to the values shown in Fig. 6 for given kr. Fast angular oscillations of the moments are due to the angular-temporal coupling of a stretched pulse. The case $C = \pm 2$, shown in Fig. 5, corresponds to doubling the laser pulse duration over one azimuthal rotation. As in our example laser pulse duration is 12 laser periods, there are 24 oscillations over one rotation. (Note that in Fig. 7 only a half of the period is shown, $\theta = 0 \div \pi$.) As the radial position corresponds to the maximum of laser pulse, the radial component of ponderomotive force is weak at this position and the radial momentum is small. By contrast, caused by the angular-temporal coupling, there are azimuthal and axial components of the ponderomotive force, $F_{\theta,z} = -\nabla_{\theta,z}|\mathbf{E}^2|$. For example, for a linearly polarized beam (3) expression for this force reads

$$F_\theta = \frac{Ct_{\rm las}}{2\pi r} a^2 f^2 g g', \qquad F_z = a^2 f^2 g g'.$$

These components attain a maximum near the laser intensity maximum in agreement with the momentum profiles shown in Fig. 6. In combination with strong azimuthal electron oscillations the azimuthal component of ponderomotive force creates an asymmetric electron shift. For this initial radial position, after averaging over the azimuthal angle, there are more particles that are gaining a negative orbital momentum, which, however, is approximately 10% of the maximum orbital momentum, as it can be seen by comparing Figs. 6a and 7c. A similar behavior is observed with radially and circularly polarized beams with a difference that the amplitude of oscillations does not depend on the azimuthal angle (not shown in the figure).

Several representative orbits of particles gaining positive and negative orbital momenta over one period of fast angular oscillations are shown in Fig. 8. Initial angles of the particle trajectories 1, 3 and 5 correspond to a zero final orbital momentum in Fig. 7c. These particles are ejected toward the laser beam axis. The particle 2 gains a positive orbital momentum and particle 4 gains a negative OAM. However, the interval between azimuthal angles corresponding to particles 1 and 3 is approximately one third of the period of fast angular oscillations in Fig. 7, while the interval between azimuthal angles corresponding

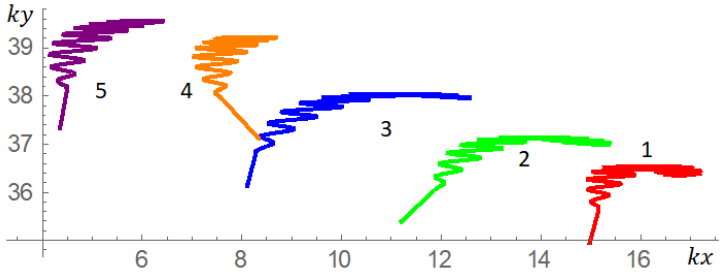

Figure 8: Electron trajectories in the transverse plane x, y in the field of a chirped laser pulse for the initial azimuthal angle $\theta_0 = 1.14$ (1, red) 1.18 (2, green), 1.25 (3, blue), 1.37 (4, purple) and 1.42 (5, purple) for the initial radius $kr_0 = 40$ and the following laser parameters: $a_0 = 1$, $kw_0 = 15\pi$, $\omega t_{\rm las} = 24\pi$, $p = 0$, $l = 1$, $C = 2$, linear polarization, x-axis corresponds to the direction of laser electric field. Particle moves from the top to the bottom.

to particles 3 and 5 is two-thirds of the period. Consequently, the average OAM is negative. All considered particles are drifting perpendicularly to the laser polarization, a small variation of the initial position affects the phase resonance between the particle and the field and consequently to a rather different final x-component of their momentum. There is no such fast nonlinear variation of particle orbits in a laser pulse without angular-temporal coupling ($C = 0$). Correspondingly, angular dependence of the orbital momentum is almost sinusoidal and it averages to a much smaller value.

The effect of enhancement of the orbital momentum transfer in a stretched laser pulse is present for all considered laser pulse amplitudes. The case $C = \pm 2$ gives an increase of orbital momentum transfer by a factor of more than twenty without changing the axial momentum P_z and by slightly decreasing the radial momentum P_r. It is therefore, a very efficient method of controlling the OAM transfer from laser beam to electrons. Efficiency of axial and orbital momentum transfer further increases in the domain of relativistic intensities: by increasing laser amplitude five times from $a_0 = 1$ to $a_0 = 5$ the OAM transfer will be increased by thousand times.

3.4. Energy distribution of accelerated electrons

A difference in the axial and orbital momenta transfer can be also understood from analysis of the distribution function of accelerated particles shown in Fig. 9 for the case of a relativistic laser pulse $a_0 = 5$ of a linear polarization with chirp $C = 2$ and without chirp. The distributions can be partially interpolated with simple exponential functions:

$$dN/dp_z \approx n_p \exp(-p_z/P_h), \qquad dN/dl_z \approx n_l \exp(-|l_z|/L_h), \tag{7}$$

with $n_p \simeq n_l$ and characteristic scales P_h and L_h, which are comparable to the average momenta $\langle p_z \rangle = P_z/\pi r_{\rm max}^2$ and $\langle l_z \rangle = L_z/\pi r_{\rm max}^2$.

In the case of non-stretched pulse, $P_h = 0.8$ and $\langle p_z \rangle = 0.41$. Laser beam stretching only slightly increases the axial momentum with $P_h = 1.3$ and $\langle p_z \rangle =$

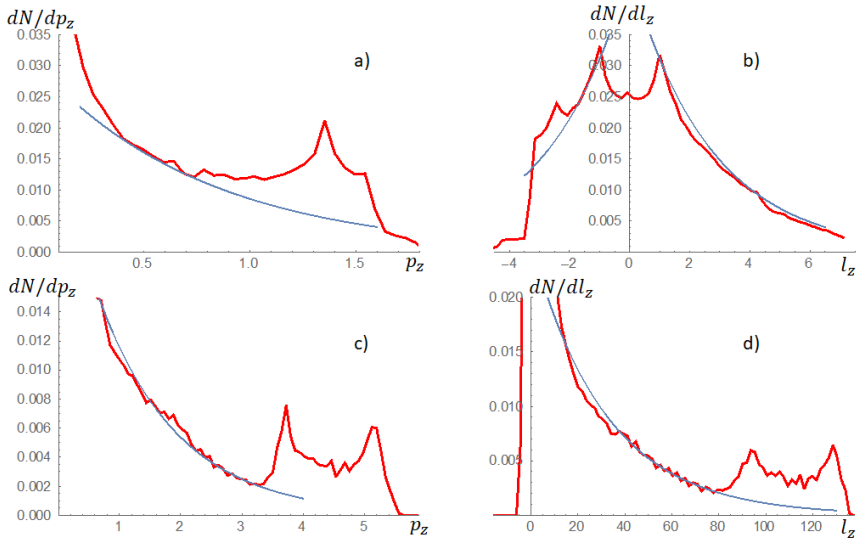

Figure 9: Distribution of accelerated particles on axial (a, c) and orbital (b, d) momentum for the following laser parameters: $a_0 = 5$, $kw_0 = 15\pi$, $\omega t_{\rm las} = 24\pi$, $p = 0$, $l = 1$, linear polarization with chirps $C = 0$ (a, b) and $C = 2$ (c, d). Solid red lines – results of numerical simulations with 40000 particles, thin blue lines – exponential interpolation with $T_h = 0.8$ (a), $L_h = 2.7$ (b), $T_h = 1.3$ (c) and $L_h = 32$ (d).

0.91. There is however, a significant difference in the orbital momentum. The number of electrons with a positive orbital momentum is much larger but in the case of non-stretched pulse $L_h \simeq 2.7$ and $\langle l_z \rangle = 0.49$ are comparable to the corresponding axial quantities. However, in a stretched pulse, the electron OAM is increased by a factor of more than ten: $L_h \simeq 32$ and $\langle l_z \rangle = 22.9$. This is an evident effect of the azimuthal component of the laser ponderomotive force facilitating the OAM transfer.

It is important to notice that in addition to a broad exponential distribution of accelerated electrons, there is a group of fast electrons that carry a large axial and orbital momentum. They are staying a long time within the pulse and are accelerated directly by the laser field.

4. Discussion and conclusions

While the simple single particle model used in this paper allows to explore a large range of laser pulse configurations, it ignores the collective plasma response and, therefore, the results presented above apply to the conditions where such collective effects can be neglected. This is the case of an underdense plasma with density much smaller than the critical density, $n_e \ll n_c$. Two types of collective effects can be considered: modification of the laser field and generation of self-considered plasma fields. The energy and momentum transfer in these conditions is small, so the depletion of laser pulse can be neglected and thus,

the laser field can be prescribed. Generation of internal plasma fields could be an important effect if the laser field is sufficiently strong and plasma density is sufficiently high. This effect has been demonstrated in full PIC simulations of laser particle interaction and momentum transfer in Refs. [7, 8, 16]. Self-consistent plasma fields confine the electrons expelled radially from the laser pulse and facilitate the axial momentum transfer. However, their effect is less significant for the orbital momentum transfer because the azimuthal plasma fields are much weaker than the axial and radial field. Consequently, we assume that the single particle model should be sufficiently accurate in laser interaction with plasmas of density smaller than 1% of the critical density.

Transfer of kinetic momentum from electromagnetic wave to particles is a fundamental process and it would be interesting to measure it experimentally. It is however very inefficient for non-relativistic laser intensities, $a_0 \leq 1$. As a figure of merit, for the reference case, 1 μm laser wavelength and plasma with an electron density $n_e \simeq 10^{19}$ cm^{-3}, that is, 1% of the critical density, the electron energy gain is ~ 1.8 J/m and rate of OAM transfer is $\sim 1.7 \times 10^{15}$ J·s/m. That means, that laser pulse will lose about 0.4% of its energy and momentum over a distance of 0.1 mm. A tighter laser focusing, increase of laser intensity and use of stretched laser pulses with angular-temporal coupling change significantly the situation. An increase of laser amplitude by five times to $a_0 = 5$ will increase the momentum transfer, both axial and orbital, by more than hundred times. By using pulse with $C = 2$ it is possible to boost the OAM transfer by twenty-thirty times more, while keeping the energy and axial momentum unchanged or even decreased. Thus, a significant part of laser OAM can be transferred to electrons over a distance less than a hundred wavelengths.

OAM transfer could be used for an efficient generation of axial magnetic fields in plasma. Electron motion is associated with electric currents and axial and azimuthal electron propagation leads to generation an azimuthal and axial magnetic fields. Using the values obtained in a single-particle approach for estimation, in relativistic dimensionless units (magnetic field is normalized by the Compton field $m_e\omega/e$), equations for the magnetic fields read:

$$\frac{dB_z}{dr} = \frac{n_e}{n_c}\frac{\bar{l}_z}{r\gamma}, \qquad \frac{d(rB_\theta)}{dr} = -\frac{n_e}{n_c}\frac{\bar{p}_z r}{\gamma}.$$

Consequently, generated magnetic field has a helical structure, which can be measured with imaging test particle propagation through the focal spot after the end of laser pulse.

The structure of magnetic field depends on the radial distribution of electron momenta. In the case of a linearly polarized and non-stretched laser pulse, according to Fig. 1b, axial and orbital moments are of the same order and are localized in a ring of radius $\sim w_0$ and width $\Delta r \sim w_0$. In this case, shown Fig. 10a for $a_0 = 5$ and $n_e/n_c = 0.01$, the axial magnetic field of a strength $B_z \sim -(n_e/n_c\gamma)\, L_z/w_0^2$ is localized essentially inside the ring of the current. By contrast, the azimuthal magnetic field is significantly stronger and it is localized outside the current ring and its intensity decreases with radius, $B_\theta \sim$

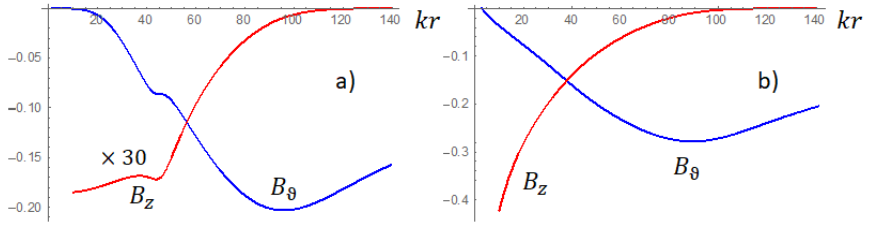

Figure 10: Radial distribution of the estimated axial (red) and azimuthal (blue) magnetic fields for the following laser parameters: $a_0 = 5$, $kw_0 = 15\pi$, $\omega t_{\rm las} = 24\pi$, $p = 0$, $l = 1$, linear polarization with $C = 0$ (a) and $C = 2$ (b). Plasma density is 1% of the critical density, axial field in panel a is multiplied by a factor of 30 for visibility.

$-(n_e/n_c\gamma)\, P_z/r$. However, in this case the azimuthal field dominates and the axial field is about 30 times weaker. The use of a stretched laser beam, as shown in Fig. 10b, does not affect the outside azimuthal magnetic field but it strongly enhances the inside axial magnetic field, which becomes of the same order as the azimuthal field. The axial magnetic field can be used for particle guiding along the laser beam axis. In the example of magnetic field distribution in a plasma shown in Fig. 10, the axial magnetic field strength is $\lesssim 0.01$ in the dimensionless units or about 50 T in the case of $C = 0$, while it increases about 50 times, that is, more than 1 kT, in the case of a stretched pulse $C = 2$. This value is larger than magnetic fields produced with optical methods in vacuum [17] and comparable to the magnetic fields in plasma proposed by other optical schemes [18].

Acknowledgments

We acknowledge PRACE for awarding us access to resource Joliot Curie-SKL based in France at TGCC Center. This work was granted access to HPC resources of TGCC under the allocation A0010506129 made by GENCI. This research was partially supported by the Czech Republic MSMT targeted support of Large Infrastructures, ELI Beamlines Project LQ1606 of the National Programme of Sustainability II. The authors acknowledge support from MEPhI Academic Excellence Project (Contract No. 02.a03.21.0005-27.08.2013).

Appendix A. Expressions for the axial components of electric and magnetic field of a focused laser pulse

Expressions for the axial components of a Laguerre–Gaussian laser beam are calculated in the first paraxial approximation (terms on the order of $1/kw_0$ and $1/\omega t_{\rm las}$) assuming div$\mathbf{E} = 0$ and div$\mathbf{B} = 0$. In the case of linear polarization

(LP) (3) we have:

$$
\begin{aligned}
E_z &= -a(z)\left(f'(r)\,g(\tau)\,\cos\theta + \frac{C}{2\pi r} f(r)\,g'(\tau)\,\sin\theta\right)\sin(l\theta+\varphi_{p,l}) \\
&+ a(z)\,f(r)\,g(\tau)\left(\frac{l}{r}\sin\theta - \frac{rz}{z_R w_b^2}\cos\theta\right)\cos(l\theta+\varphi_{p,l}), \qquad \text{(A.1)} \\
B_z &= -a(z)\left(f'(r)\,g(\tau)\,\sin\theta - \frac{C}{2\pi r} f(r)\,g'(\tau)\,\cos\theta\right)\sin(l\theta+\varphi_{p,l}) \\
&- a(z)\,f(r)\,g(\tau)\left(\frac{l}{r}\cos\theta + \frac{rz}{z_R w_b^2}\sin\theta\right)\cos(l\theta+\varphi_{p,l}), \qquad \text{(A.2)}
\end{aligned}
$$

where f' and g' are derivatives of functions f and g over their respective arguments.

Similarly, for a circularly polarized (CP) laser pulse (4), the axial field components write:

$$
\begin{aligned}
E_z &= -\frac{a(z)}{\sqrt{2}}\left(f'(r) - s\frac{l}{r}f(r)\right)\,g(\tau)\,\sin[(l+s)\theta+\varphi_{p,l}] \\
&+ \frac{a(z)}{\sqrt{2}}\,f(r)\left(\frac{s\,C}{2\pi r}g'(\tau) - \frac{rz}{z_R w_b^2}g(\tau)\right)\cos[(l+s)\theta+\varphi_{p,l}], \qquad \text{(A.3)} \\
B_z &= \frac{a(z)}{\sqrt{2}}\left(s\,f'(r) - \frac{l}{r}f(r)\right)\,g(\tau)\,\cos[(l+s)\theta+\varphi_{p,l}] \\
&+ \frac{a(z)}{\sqrt{2}}\,f(r)\left(\frac{C}{2\pi r}g'(\tau) - s\frac{rz}{z_R w_b^2}g(\tau)\right)\sin[(l+s)\theta+\varphi_{p,l}]. \qquad \text{(A.4)}
\end{aligned}
$$

For a radially polarized (RP) laser pulse (5), the axial field components write:

$$
\begin{aligned}
E_z &= -a(z)\left[\left(f'(r) + \frac{1}{r}f(r)\right)\,g(\tau)\,\cos\alpha + \frac{C}{2\pi r}f(r)\,g'(\tau)\,\sin\alpha\right]\sin(l\theta+\varphi_{p,l}) \\
&+ a(z)\,f(r)\,g(\tau)\left(\frac{l}{r}\sin\alpha - \frac{rz}{z_R w_b^2}\cos\alpha\right)\cos(l\theta+\varphi_{p,l}), \qquad \text{(A.5)} \\
B_z &= -a(z)\left[\left(f'(r) + \frac{1}{r}f(r)\right)\,g(\tau)\,\sin\alpha - \frac{C}{2\pi r}f(r)\,g'(\tau)\,\cos\alpha\right]\sin(l\theta+\varphi_{p,l}) \\
&- a(z)\,f(r)\,g(\tau)\left(\frac{l}{r}\cos\alpha + \frac{rz}{z_R w_b^2}\sin\alpha\right)\cos(l\theta+\varphi_{p,l}). \qquad \text{(A.6)}
\end{aligned}
$$

Appendix B. Results of numerical simulations of momentum and energy transfer

Here we present for reference the results of numerical simulations of single particle motion averaged over the azimuthal and radial initial positions.

a_0	l	P_z	L_z
0.1	0	0.245	0
0.3	0	3.16	0
1.0	0	154	0
3.0	0	8.04×10^3	0
10.0	0	1.18×10^5	0
0.1	1	0.144	0.424
0.3	1	2.08	3.98
1.0	1	96.0	125
3.0	1	5.41×10^3	6.26×10^3
10.0	1	1.12×10^5	1.31×10^5
0.1	2	0.157	0.625
0.3	2	1.48	6.19
1.0	2	62.8	161
3.0	2	4.04×10^3	8.29×10^3
10.0	2	1.16×10^6	2.52×10^5

Table B.2: Dependence of the axial and orbital momenta of electron on the laser amplitude varying from $a_0 = 0.1$ to $a_0 = 10$ for a linearly polarized beam with the following parameters: $kw_0 = 15\pi$, $\omega t_{\rm las} = 24\pi$, $p = 0$ and $C = 0$. Electron energy is approximately equal to the axial momentum.

C	l	P_z	L_z	$\mathcal{E}_e$
0	-1	103	-87.3	103
0	0	143	64.7	143
0	1	79.7	144	79.7
0	2	62.8	203	62.8
-2.5	1	56.1	2150	79.1
-2.0	1	44.5	1700	83.5
-1.5	1	56.1	766	81.0
-1.0	1	73.5	99.2	80.4
-0.5	1	79.1	48.1	79.8
0.5	1	79.1	393	79.8
1.0	1	74.7	414	77.9
1.5	1	58.6	207	78.5
2.0	1	44.5	-605	79.8
2.5	1	52.4	-929	74.7

Table B.3: Dependence of the axial and orbital momenta of electron and its energy on the laser orbital momentum l and stretching parameter C for a circularly polarized beam with the following parameters: $a_0 = 1$, $kw_0 = 15\pi$, $\omega t_{\rm las} = 24\pi$ and $p = 0$. Some data are shown in Fig. 2.

References

[1] L. Allen, M. W. Beijersbergen, R. J. C. Spreeuw, and J. P. Woerdman. Orbital angular momentum of light and the transformation of laguerre-gaussian laser modes. *Phys. Rev. A*, 45:8185, 1992.

C	l	α	P_z	L_z	$\mathcal{E}_e$
0	0	0	250	0	250
0	1	0	79.8	148	79.8
0	1	0.1π	79.8	121	79.8
0	1	0.2π	80.4	84.2	80.4
0	1	0.25π	79.8	67.2	79.8
0	1	0.3π	79.8	52.9	79.8
0	1	0.4π	79.8	38.2	79.8
0	1	0.5π	79.1	46.0	79.1
0	1	0.6π	79.1	73.5	79.1
0	1	0.7π	79.1	110	79.1
0	1	0.8π	79.1	142	79.1
0	1	0.9π	79.8	156	79.8
-2.5	1	0	78.5	-1700	79.1
-2.0	1	0	78.5	-1290	79.1
-1.5	1	0	78.5	-898	79.1
-1.0	1	0	79.8	-539	80.4
-0.5	1	0	78.5	143	79.1
0.5	1	0	78.5	490	79.1
1.0	1	0	79.8	835	80.4
1.5	1	0	78.5	1200	79.1
2.0	1	0	78.5	1590	78.5
2.5	1	0	78.5	2000	79.1

Table B.4: Dependence of the axial and orbital momenta of electron and its energy on the laser orbital momentum, polarization angle and angular-temporal coupling parameter for a radially polarized beam with the following parameters: $a_0 = 1$, $kw_0 = 15\pi$, $\omega t_{\rm las} = 24\pi$ and $p = 0$. Some data are shown in Fig. 2.

[2] Q. Zhan. Cylindrical vector beams: from mathematical concepts to applications. *Adv. Opt. Photon.*, 1:1, 2009.

[3] J. Vieira and J. T. Mendonça. Nonlinear laser driven donut wakefields for positron and electron acceleration. *Phys. Rev. Lett.*, 112:215001, 2014.

[4] J. Vieira, R. M. G. M. Trines, E. P. Alves, R. A. Fonseca, J. T. Mendonça, R. Bingham, P. Norreys, and L. O. Silva. Amplification and generation of ultra-intense twisted laser pulses via stimulated raman scattering. *Nature Commun.*, 7:10371, 2016.

[5] J. Vieira, J. T. Mendonça, and F. Quéré. Optical control of the topology of laser-plasma accelerators. *Phys. Rev. Lett.*, 121:054801, 2018.

[6] Y. Shi, J. Vieira, R. M. G. M. Trines, R. Bingham, B. F. Shen, and R. J. Kingham. Magnetic field generation in plasma waves driven by co-propagating intense twisted lasers. *Phys. Rev. Lett.*, 121:145002, 2018.

[7] C. Baumann and A. Pukhov. Electron dynamics in twisted light modes of relativistic intensity. *Phys. Plasmas*, 25:083114, 2018.

[8] R. Nuter, Ph. Korneev, I. Thiele, and V. T. Tikhonchuk. A plasma solenoid driven by a laser beam carrying an orbital angular momentum. *Phys. Rev. E*, 98:033211, 2018.

[9] D. R. Blackman, R. Nuter, Ph. Korneev, and V. T. Tikhonchuk. Kinetic plasma waves carrying an angular momentum. *Phys. Rev. E*, 100:013204, 2019.

[10] G. Malka, E. Lefebvre, and J.-L. Miquel. Experimental observation of electrons accelerated in vacuum to relativistic energies by a high-intensity laser. *Phys. Rev. Lett.*, 78:3314, 1997.

[11] P. X. Wang, Y. K. Ho, X. Q. Yuan, Q. Kong, N. Cao, L. Shao, A. M. Sessler, E. Esarey, E. Moshkovich, Y. Nishida, N. Yugami, H. Ito, J. X. Wang, and S. Scheid. Characteristics of laser-driven electron acceleration in vacuum. *J. App. Phys.*, 91:856, 2002.

[12] A. P. L. Robinson, A. V. Arefiev, and D. Neely. Generating "superponderomotive" electrons due to a non-wake-field interaction between a laser pulse and a longitudinal electric field. *Phys. Rev. Lett.*, 111:065002, 2013.

[13] P. M. Woodward. A method of calculating the field over a plane aperture required to produce a given polar diagram. *J. Inst. Electr. Eng. Part 1*, 93:1554, 1947.

[14] J. D. Lawson. Lasers and accelerators. *IEEE Trans. Nucl. Sci.*, NS-26:4217, 1979.

[15] G. Pariente and F. Quéré. Spatio-temporal light springs: extended encoding of orbital angular momentum in ultrashort pulses. *Opt. Lett.*, 40:2037, 2015.

[16] R. Nuter, Ph. Korneev, E. Dmitriev, I. Thiele, and V. Tikhonchuk. Electron orbital angular momentum gain in a direct laser acceleration process. *Phys. Rev. E*, submitted, 2020.

[17] J. J. Santos, M. Bailly-Grandvaux, M. Ehret, A. V. Arefiev, D. Batani, F. N. Beg, A. Calisti, S. Ferri, R. Florido, P. Forestier-Colleoni, S. Fujioka, L. Giuffrida, L. Gremillet, J. J. Honrubia, S. Kojima, Ph. Korneev, K. F. F. Law, J.-R. Marquès, A. Morace, C. Mossé, O. Peyrusse, S. Rose, M. Roth, S. Sakata, G. Schaumann, F. Suzuki-Vidal, V. T. Tikhonchuk, T. Toncian, N. Woolsey, and Z. Zhang. Laser-driven strong magnetostatic fields with applications to charged beam transport and magnetized high energy-density physics. *Phys. Plasmas*, 25:056705, 2018.

[18] P. Korneev, E. d'Humières, and V. Tikhonchuk. Gigagauss-scale quasistatic magnetic field generation in a snail-shaped target. *Phys. Rev. E*, 91:043107, 2015.